Supporting Information

Green Synthesis of Oxygenic Graphyne with High Electrochemical Performance from Efficient Mechanochemical Degradation of Hazardous Decabromodiphenyl Ether

***Yingjie Li*[*, †], Xiaoyu Wang[†], Bo Qiang[†], Shenao Xu[†], Jing Gu[†], Xiaojun He[†], Chunxi Li*[*, ‡]**

[†] Anhui Key Lab of Coal Clean Conversion and Utilization, School of Chemistry and Chemical Engineering, Anhui University of Technology, Maanshan 243032, P. R. China

[‡] State Key Laboratory of Chemical Resource Engineering, College of Chemical Engineering, Beijing University of Chemical Technology, Beijing 100029, P. R. China

*Corresponding Author

Yingjie Li (liyingjie0408@163.com) & Chunxi Li (licx@mail.buct.edu.cn)

Table of Contents

Experimental Section ----------S3
Mechanochemical reaction process of CaC_2 and BDE-209----------S3
Characterization instruments ----------S5
Electrochemical performance measurements ----------S6
Figure S1. Appearance changes during this mechanochemical reaction ----------S4
Figure S2. The standard XRD spectra of the related materials ----------S8
Figure S3. The standard FTIR spectrum of the used BDE-209----------S9
Figure S4. The superiority of the mechanochemical strategy ----------S10
Figure S5. BDE-209 degradation under different rotate speed with different milling time ----------S11
Figure S6. BDE-209 degradation under different reactant proportion with different milling time---S12
Figure S7. Additional SEM images of oxygenic graphyne at different magnifications----------S16
Figure S8. Additional TEM and HRTEM images of oxygenic graphyne----------S17
Figure S9. CV curves of the oxygenic graphyne electrode at different scan rates----------S19
Figure S10. GCD curves of the oxygenic graphyne electrode at different current densities ----------S20
Table S1. Detailed data and carbon balance of the mechanochemical reaction process----------S3
Table S2. The consumption analysis for mechanochemical degradation of BDE-209----------S13
Table S3. Compositional results obtained from EA, XPS, and EDS analysis----------S14
Table S4. The detailed results for the N_2 adsorption–desorption analysis ----------S15
Table S5. The fitting results of the XPS C1s and O1s narrow scan----------S18
Table S6. Cm and Cv values of the oxygenic graphyne from CV and GCD curves----------S21
Table S7. Comparison of various carbon electrode materials for supercapacitors----------S22
Table S8. The electrical conductivity performance of various carbon materials----------S23
References ----------S24

Experimental Section

Mechanochemical reaction process of CaC_2 and BDE-209

Before reaction, bulk CaC_2 was pulverized into powder by a high speed crusher, then the powder was screened by 100 mesh sieve, and sealed for latter use. In this work, a planetary ball mill with four 250 mL zirconia lined stainless steel mill pot contained approximately 350 g zirconia balls with three different diameters (175 g-5 mm, 105 g-8 mm, and 70 g-10 mm) was used. The detailed analysis results for the mechanochemical reaction under 150 min, 700 rpm and CaC_2:BDE-209=15 (three times of the stochiometric ratio) are listed in **Table S1**. **Figure S1** shows the appearance changes of the mixture before and after reaction, i.e. from off-white to bright black. In addition, the main influence factors on the BDE-209 degradation efficiency were investigated, including milling time, rotate speed and reactant ratio.

Table S1. Detailed data and carbon balance of the mechanochemical reaction process.

		Dosage	Carbon balance/g
Input	CaC_2 (80 wt%)	17.08*75%=12.81 g/0.200 mol	4.80 g
	BDE-209	13.35*99%=13.22 g/0.014 mol	1.99 g
	Total	**22.21 g**	**6.79 g**
Theoretical output	Pure CaC_2	8.35 g	3.15 g
	BDE-209	0	0
	oxygenic graphyne	3.86 g	3.64 g
	$CaBr_2$	13.78 g	0
	Total	**22.21 g**	**6.79 g**
Experimental output	Pure CaC_2 (C_2H_2)[a]	7.90 g (3151 mL)	2.96 g
	BDE-209[b]	~0	~0
	oxygenic graphyne[c]	4.02 g	3.49 g
	$CaBr_2$ (Br^-)[d]	13.58 g (10.86 g)	0
	Total	**22.21 g**	**6.75 g**

[a] The CaC_2 and reletive C amount were calculated by the produced volume of C_2H_2 from the mixture hydrolyzation.

[b] BDE-209 was undetectable by HPLC in the resulting mixture.

[c] The carbon content in oxygenic graphyne was obtained from EA analysis.

[d] Amounts of Br^- in the filtrate was detected by IC.

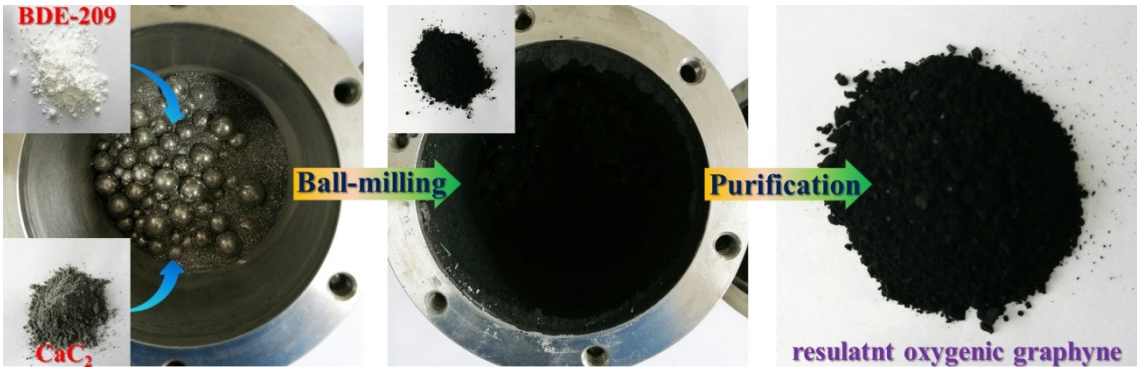

Figure S1. Appearance change of the reactant mixture before and after reaction

---

The residue BDE-209 and the resultant Br^- in the milled mixture were analyzed as follows. First, for the analysis of the residue BDE-209 in the milled mixture, 0.1 g of powder was sampled and extracted by 20 g tetrahydrofuran along with ultrasonic treatment for 30 min. The resulting solution was centrifugalized at 7000 rpm for 5 min, and the supernatant was analyzed using a high performance liquid chromatography (Shimadzu, LC2030) equipped with a UV detector with a wavelength of 300 nm and C-18 column. 1 μL of the sample is injected in the split mode by an auto-sampler, and the mobile phase is a mixture of tetrahydrofuran and methanol with a volume ratio of 90:10. The destruction degree of BDE-209 was calculated as follows:

$$Destruction\ degree = \frac{m - M \times C}{m} \times 100\%$$

Here, m is the theoretical addition mass of BDE-209 in the sample, M is the mass of the tetrahydrofuran, and C is the BDE-209 content in the solution.

The bromine of BDE-209 is mineralized to Br^- via mechanochemical reaction, and finally went into the filtrate after pickling and washing processes. The Br^- content in the filtrate was analyzed by ICS-900 ion chromatography (DIONEX, China). The debromination degree of BDE-209 was calculated as follows:

$$Debromination\ degree = \frac{M \times C}{m \times 83.306\%} \times 100\%$$

Here, M is the mass of the filtrate, C is the Br^- content in the filtrate, m is the mass of BDE-209 used in the reaction, and 83.306% is the organic bromine content in BDE-209.

In addition, the application performance of the mechanochemical strategy were evaluated for BDE-209-containing (as flame retardant) PE, PP, PS and PA6 products under 60 min, 550 rpm and CaC_2:BDE-209=15. For this part, the content of BDE-209 in the related products conforms to the current conventional industrial addition, i.e., 25%, 25%, 10% and 15% for PE, PP, PS and PA6 respectively. In order to maintain a consistent pellet ratio, the total mass of the added material in the mill pot does not exceed 25 g.

Characterization instruments

Element analysis (EA) was done by a vario EL cube instrument (Elementar, Germany). The X-ray energy-dispersive spectroscopy (EDS) was recorded on an X-MaxN 80T system (OXFORD Instruments, UK). Scanning electron microscopy (SEM) images were recorded on a NANO SEM430 microscope (ThermoFisher Scientific, US). N_2 adsorption-desorption isotherm was obtained at 77 K with a computer-controlled N_2 gas adsorption analyzer (Micromeritics, US). Brunauer-Emmett-Teller (BET) and density functional theory (DFT) methods were employed for the determination of specific surface area and pore size distribution, respectively. High-resolution transmission electron microscopy (HR-TEM) images were recorded on a JEM-2100 microscope (Hitachi, Japan). X-ray diffraction (XRD) was conducted using a Bruker D8 Advance XRD system (BRUKER, Germany) with Cu Kα radiation at 5° min^{-1} in the 2θ range of 10°~70°. Atomic force microscopy (AFM) images were recored on NanoMan VS scanning probe microscope (BRUKER, Germany). Raman spectrum was recorded on a Raman microscope (Renishaw, UK) under an excitation of 532 nm. X-ray photoelectron spectroscopy (XPS) was done on a Thermo Escalab 250Xi instrument (Thermo Electron, US).

Electrochemical performance measurements

The working electrodes were fabricated by mixing the oxygenic graphyne and polytetrafluoroethylene (PTFE) in a mass ratio of 9:1 in ethanol. Notably, no conductive filler (e.g., acetylene black) was used because of the high conductivity of the oxygenic graphyne. Then, the mixture was rolled into sheets and pressed on nickel foam current collector with a coating area of 1 cm^2. Finally, the as-fabricated electrode was dried at 120 °C for 10 h in a vacuum oven for the complete removal of ethanol. Dry electrode was assembled as symmetric supercapacitors in a three-electrode cell with platinum foil and Hg/HgO electrodes as the counter and reference electrode, respectively. A 6 M KOH solution was used as the electrolyte.

CV, GCD and EIS investigations were conducted on a CHI 660E electrochemical workstation (Chenhua Instrument, Shanghai, China). CV tests were investigated between -1.0 and 0 V (vs. Hg/HgO) at scan rates ranging from 1 to 100 mV s^{-1}. GCD test was conducted at the same potential range at current densities ranging from 0.2 to 20.0 A g^{-1}. EISs were characterized at open-circuit potential in the frequency range from 100 kHz to 0.01 Hz with amplitude of 5 mV. The long cycling performance was conducted by GCD method under 4.0 A g^{-1} at the same potential range on a LANHE battery-testing instrument (LAND Electronics Co., Ltd., Wuhan, China).

The gravimetric specific capacitance (C_m, F g^{-1}) and volumetric specific capacitance (C_v, F cm^{-1}) of the electrode were calculated using CV and GCD curves. On the basis of the CV curves, the C_m value of the electrode at various scan rates was calculated as follows:

$$C_m = \frac{\int IdV}{2mv\Delta V}$$

where m is the mass of the oxygenic graphyne (g), ν is the potential scan rate (V s^{-1}), ΔV is the range of potential (V), I is the response current (A), and $\int IdV$ is the mathematical integral of the CV curve.

Based on the GCD curves, the C_m value of the electrode at various current densities was calculated as follows:

$$C_m = \frac{I\Delta t}{m\Delta V}$$

where m is the mass of the oxygenic graphyne (g), I is the charge/discharge current (A), ΔV is the potential range of charge/discharge (V), and Δt is the discharge time (s).

The C_v values of the oxygenic graphyne electrode were calculated as follows:

$$C_v = C_m \times \rho$$

where C_m is the gravimetric specific capacitance (F g^{-1}), ρ is the density of the oxygenic graphyne (1.22 g cm^{-3}).

The relaxation time (τ_0, s) of the electrode was calculated from Bode plot as follows:

$$\tau_0 = 1/f_0$$

where f_0 is the characteristic frequency of oxygenic graphyne at the phase angle of -45°.

Besides, electrical conductivity of the oxygenic graphyne was measured using AC 4-probe method on a RTS-9 dual electric 4-probe tester (4-Probe Technology Ltd, Guangzhou, China). Before test, the power was pressed to sheet with a pressure of 15 MPa.

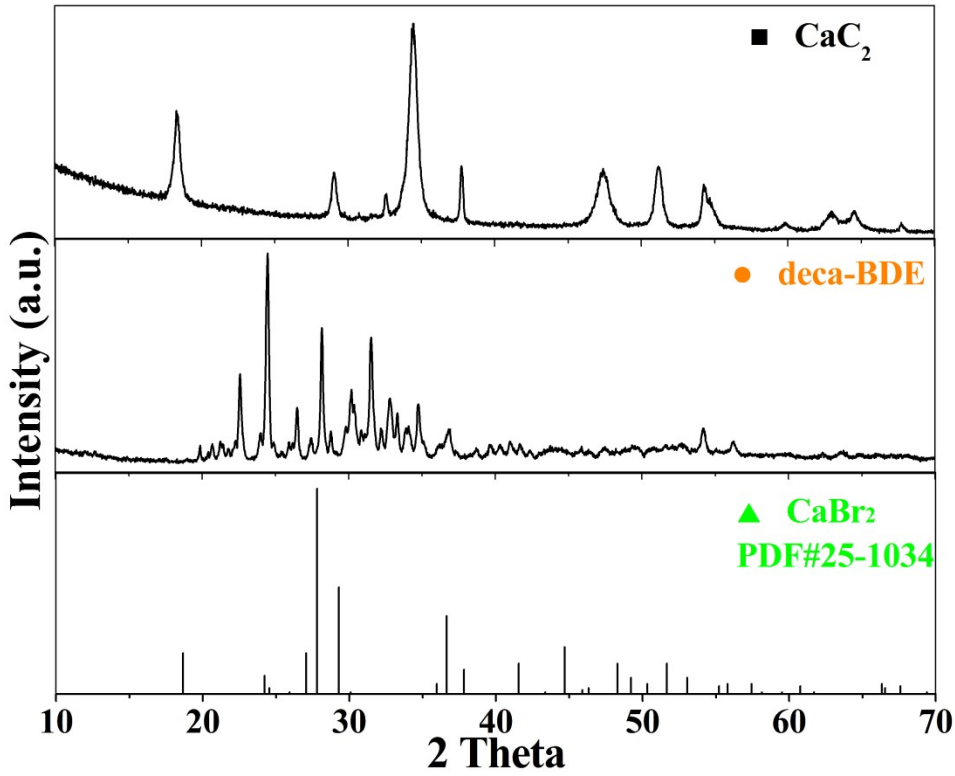

Figure S2. The XRD spectra of the related materials.

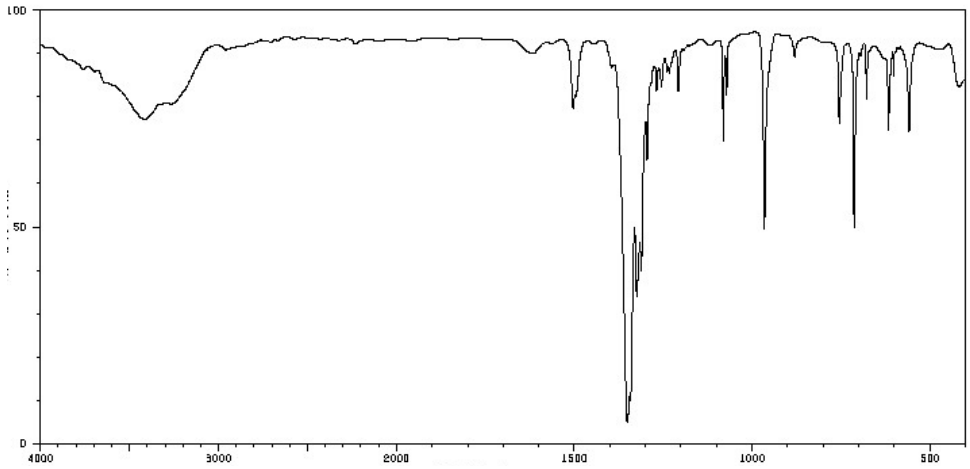

Figure S3. The standard FTIR spectrum of BDE-209. (Reproduced with permission from the Chemical Database of Chinese Academy of Sciences)

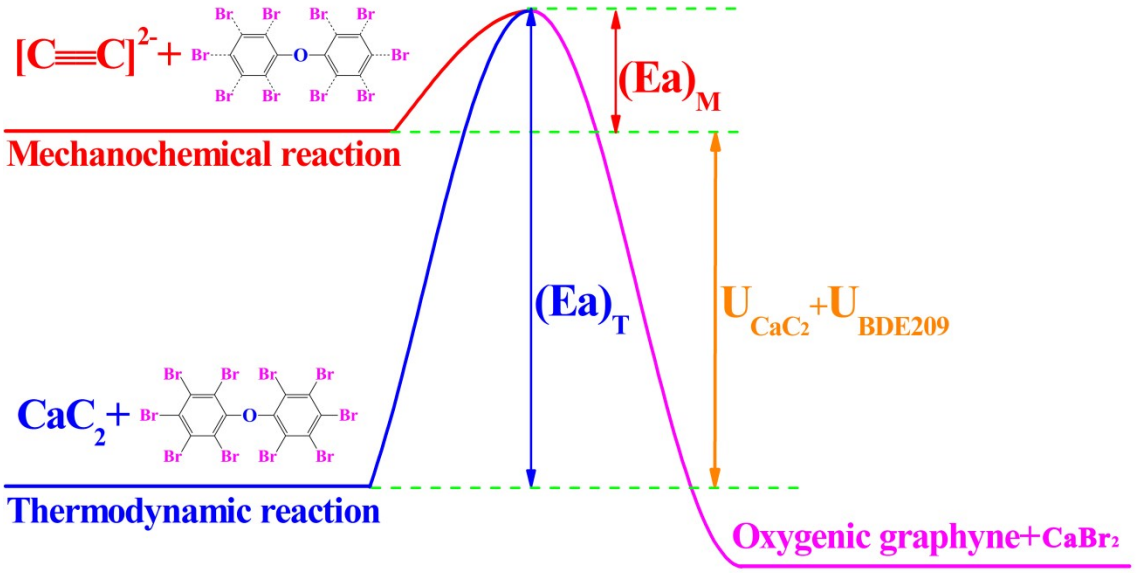

Figure S4. The superiority of the mechanochemical versus thermodynamic reactions.

Compared with thermal reaction, mechanochemistry can significantly reduce the activation energy of the reaction between BDE-209 and CaC_2, due to its dynamic miniturization for the solid reactants. As shown in **Figure S4**, the activation energy [$(Ea)_T$] for the thermodynamic reaction is extremely high due to the huge lattice energies of the bulk solid of CaC_2 and BDE-209. Thus , the reaction is very difficult to occur or require harsh thermal reaction conditions. However, mechanochemistry can remarkably excite the reactivity of the solid reactants via breaking the lattice energy dynamically, which dramatically lowers the energy barrier of the solid-solid reaction, or the mechanochemical activation energy [$(Ea)_M$]. Thus, mechanochemistry shows great superiority over thermochemistry in this process.

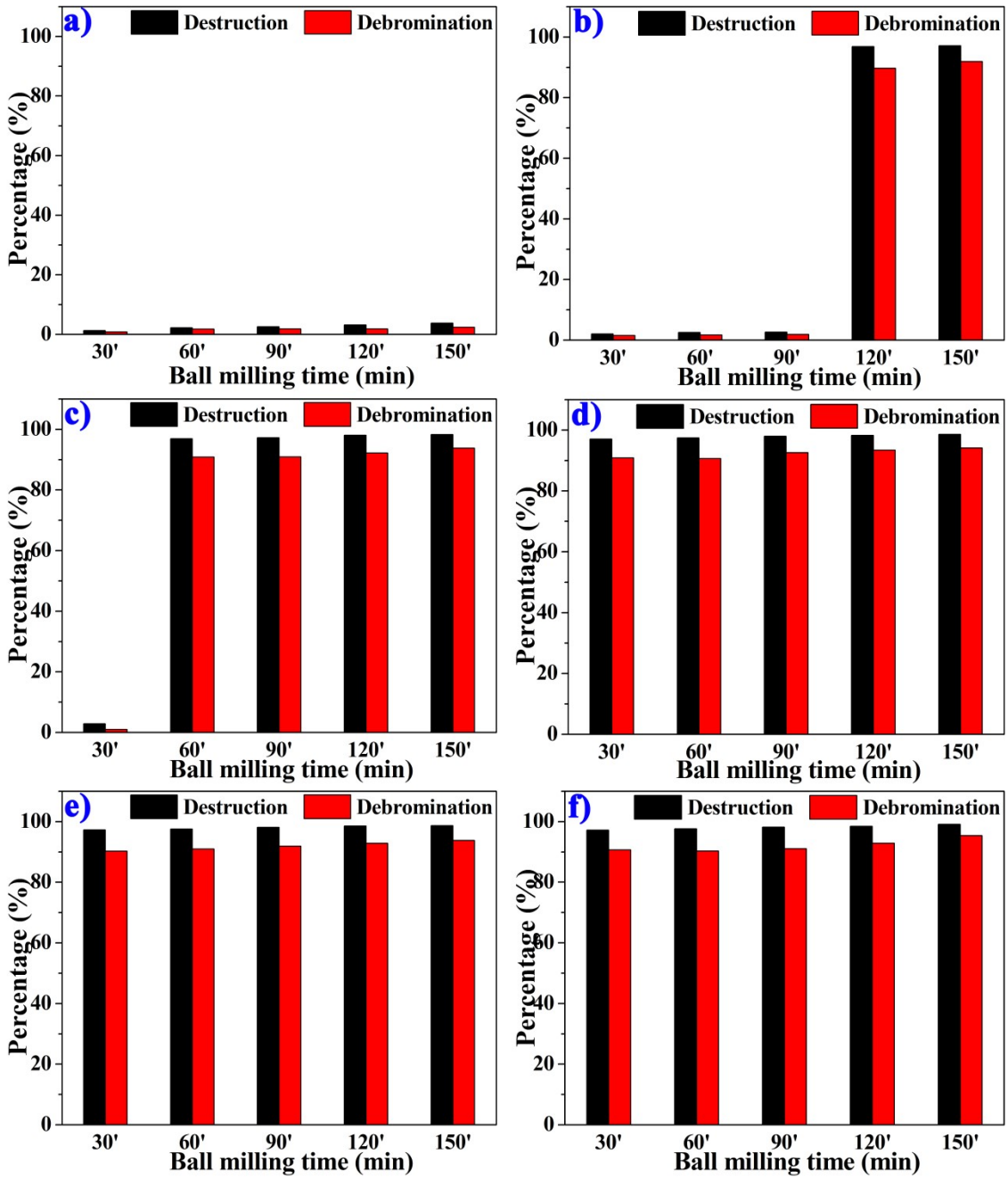

Figure S5. BDE-209 degradation under different rotate speed and milling time at CaC_2:BDE-209=15. (a) 400 rpm; (b) 450 rpm; (c) 500 rpm; (d) 550 rpm; (e) 600 rpm; (d) 650 rpm.

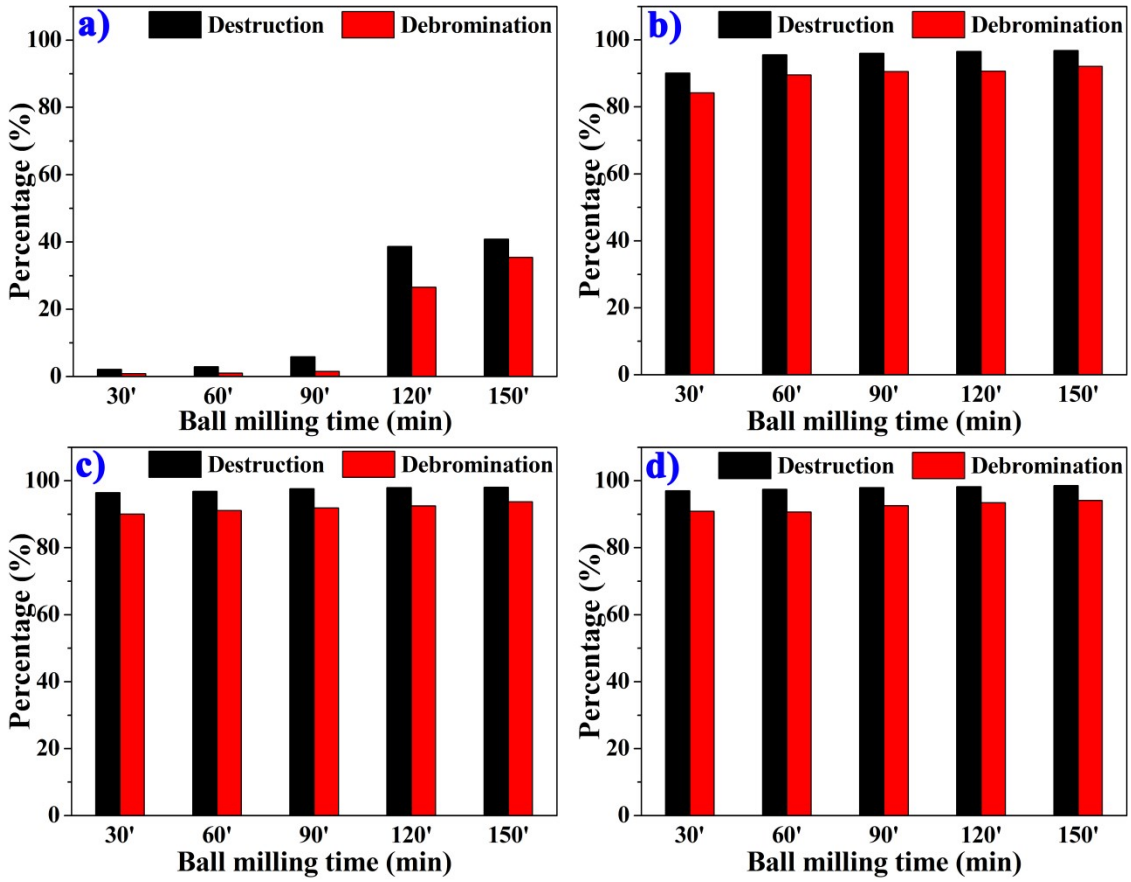

Figure S6. BDE-209 degradation under different reactant ratio and milling time at rotate speed of 550 rpm. (a) CaC_2:BDE-209=2.5; (b) CaC_2:BDE-209=5; (c) CaC_2:BDE-209=10; (d) CaC_2:BDE-209=15.

Table S2. The consumption analysis for mechanochemical degradation of BDE-209 under several typical experimental conditions.

Experiment condition setting	BDE209 Destruction (%)	BDE209 Debromination (%)	Consumption details						Total (¥)
			Raw materials		Energy consumption (¥0.65/kWh)[d]		Auxiliary materials		
			BDE209[a]	CaC_2 (¥3/kg)[d]	Ball milling[b]	Drying[c]	H_2O (¥2/kg)[d]	HCl (31%, ¥0.2/kg)[d]	
120 min, 450 rpm, CaC_2:BDE209=15	96.8	89.7	1.0 kg	1.28 kg	1.24 kWh	2.88 kWh	6 kg	4.71 kg	19.5
			/	¥3.84	¥0.80	¥1.87	¥12.0	¥0.94	
60 min, 500 rpm, CaC_2:BDE209=15	96.9	90.8	1.0 kg	1.28 kg	0.69 kWh	2.88 kWh	6 kg	4.71 kg	19.1
			/	¥3.84	¥0.45	¥1.87	¥12.0	¥0.94	
30 min, 550 rpm, CaC_2:BDE209=15	97.1	90.9	1.0 kg	1.28 kg	0.38 kWh	2.88 kWh	6 kg	4.71 kg	18.9
			/	¥3.84	¥0.25	¥1.87	¥12.0	¥0.94	
60 min, 550 rpm, CaC_2:BDE209=5	95.5	90.0	1.0 kg	0.43 kg	0.76 kWh	2.88 kWh	2 kg	1.58 kg	8.0
			/	¥1.28	¥0.49	¥1.87	¥4.0	¥0.32	
90 min, 600 rpm, CaC_2:BDE209=15	98.1	91.9	1.0 kg	1.28 kg	1.24 kWh	2.88 kWh	6 kg	4.71 kg	19.5
			/	¥3.84	¥0.80	¥1.87	¥12.0	¥0.94	
30 min, 550 rpm, CaC_2:BDE209=10	96.5	90.1	1.0 kg	0.86 kg	0.38 kWh	2.88 kWh	3 kg	3.16 kg	11.3
			/	¥2.56	¥0.25	¥1.87	¥6.0	¥0.63	
150 min, 550 rpm, CaC_2:BDE209=10	98.1	93.8	1.0 kg	0.86 kg	1.89 kWh	2.88 kWh	3 kg	3.16 kg	12.3
			/	¥2.56	¥1.23	¥1.87	¥6.0	¥0.63	

[a] Data in the table are calculated per kilogram of BDE-209 degradated;

[b] Calculating basis for energy consumption of ball milling: rated power of ball mill reactor is 1.1 kW and its maximum rotate speed is 800 rpm;

[c] Calculating basis for energy consumption of drying: rated power of vacuum drier is 1.2 kW with highest use temperature of 250 °C;

[d] The prices of materials and electricity is based on the official local pricing.

Table S3. Compositional results obtained from EA, EDS, and XPS analysis.

Technological means	Element content in oxygenic graphyne (wt%)				
	C	**O**	**Br**	**Ca**	∑
EA	86.7	5.4	0.6[a]	/	90.6
EDS	92.9	5.3	1.8	/	100.0
XPS	93.2	5.4	0.8	0.6	

[a] The residual bromine in the obtained oxygenic graphyne was measured by ion chromatography through oxygen flask combustion method.

Table S4. The detailed results for the N_2 adsorption-desorption analysis.

S_{BET} (m^2 g^{-1})	S_{mic} (m^2 g^{-1})	V_{total} (cm^3 g^{-1})	V_{mic} (cm^3 g^{-1})	V_{mes} (cm^3 g^{-1})	D_{ap} (nm)
567	118	0.82	0.16	0.66	5.7

S_{BET}: specific surface area obtained by the BET method;

S_{mic}: micropore specific surface area;

V_{total}: total pore volume;

V_{mic}: micropore volume;

V_{mes}: mesopore volume;

D_{ap}: average pore diameter.

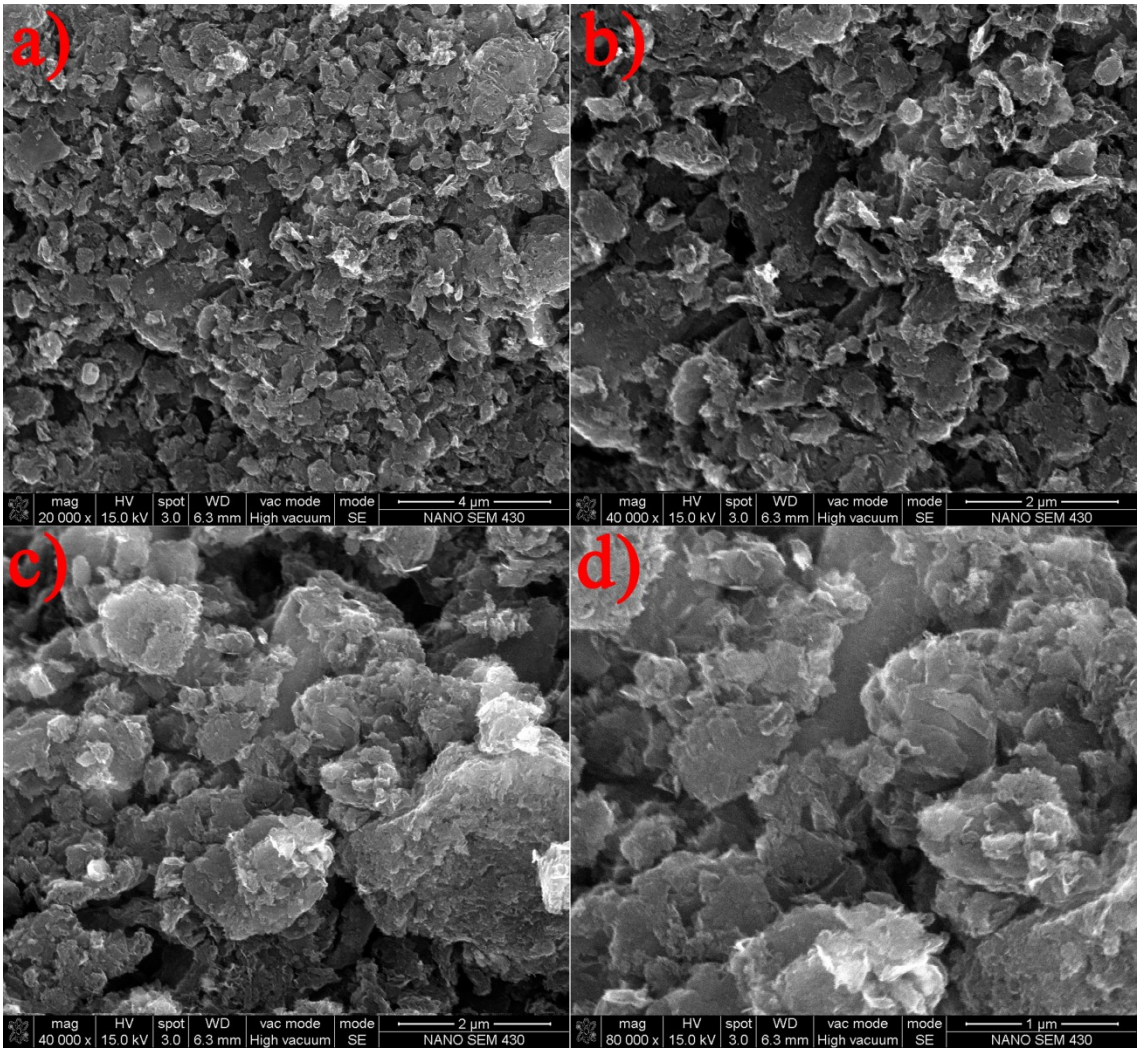

Figure S7. Additional SEM images of oxygenic graphyne at different magnifications.

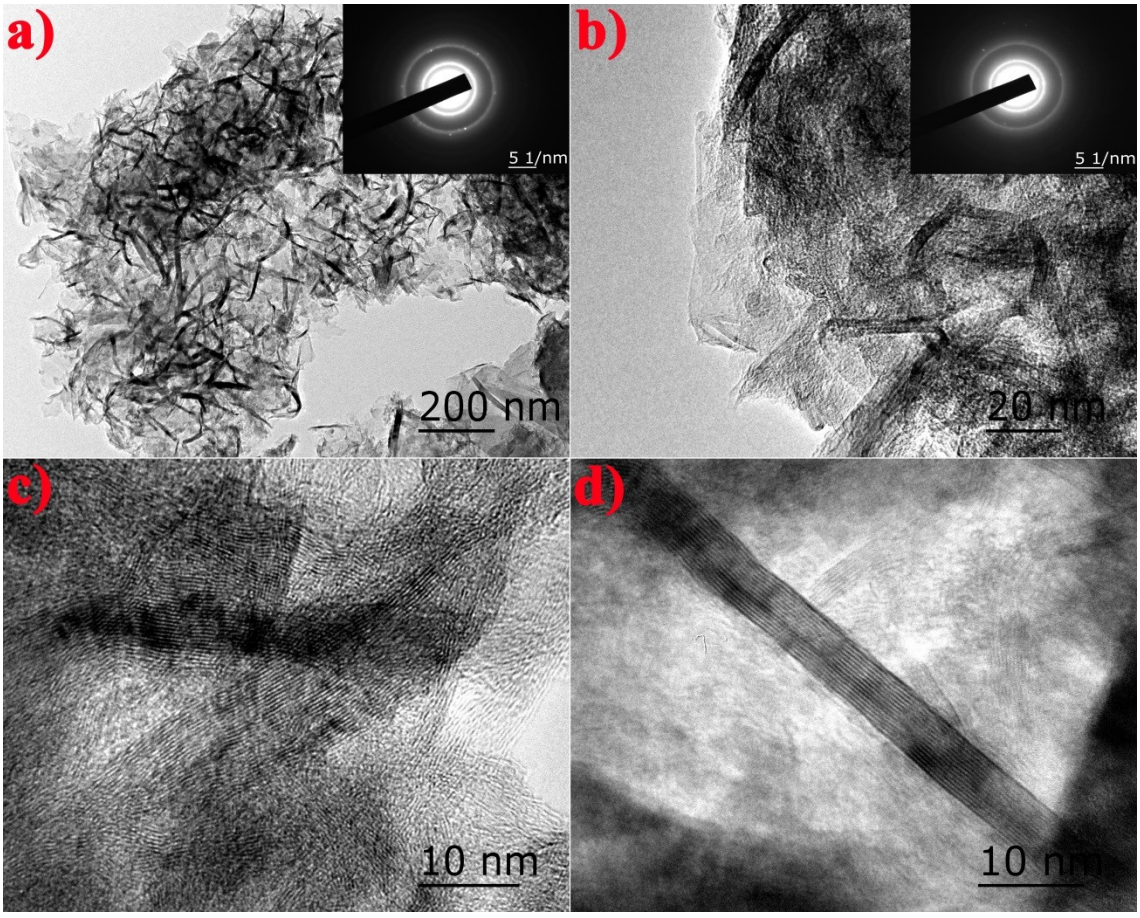

Figure S8. Additional TEM and HRTEM images of the oxygenic graphyne.

Table S5. The fitting results of the XPS C 1s and O 1s narrow scan.

Element	Carbon bond	Position (eV)	FWHM	Area ratio (%)
C 1s	C–C (sp^2)	284.4	0.6	48.6
	C–C (sp)	285.0	1.7	37.9
	C–O	286.6	1.5	7.6
	C=O	288.8	3.5	5.8
O 1s	C=O	531.0	2.0	14.3
	C–OH/C–O–C	532.3	2.9	48.7
	O–C=O	533.5	1.9	37.0

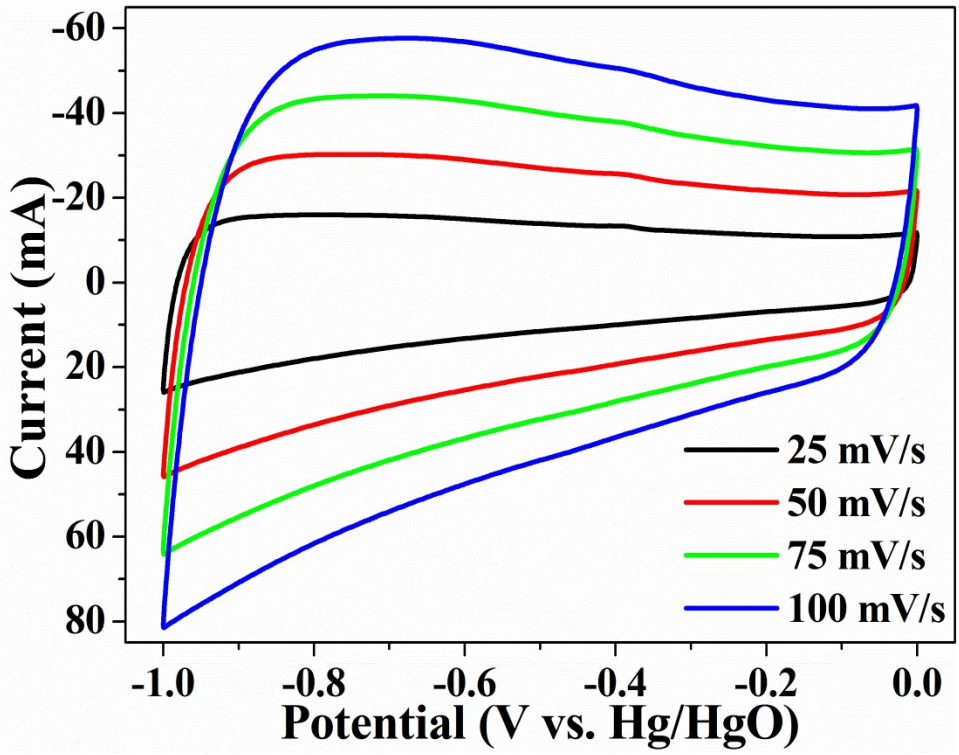

Figure S9. CV curves of the oxygenic graphyne electrode at different scan rates ranging from 25 to 100 mV s^{-1} in the potential range between -1.0 and 0 V (vs. Hg/HgO). The C_m and C_v values derived from the CV curves are listed in **Table S6**.

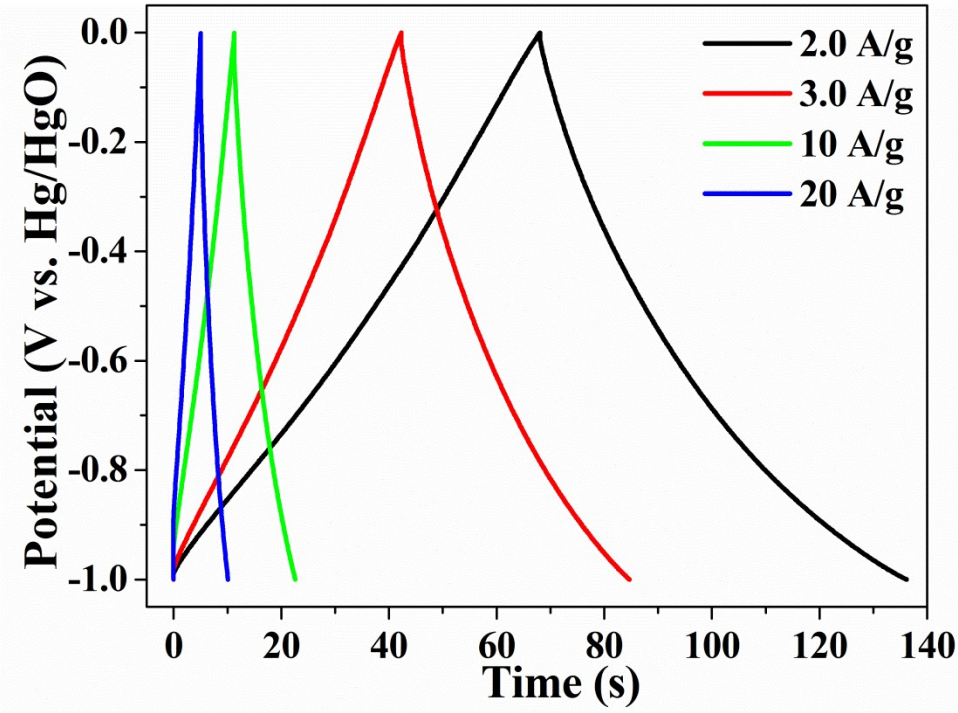

Figure S10. GCD curves of the oxygenic graphyne electrode at different current densities ranging from 2 to 20 A g^{-1} in the potential range between -1.0 and 0 V. The C_m and C_v values derived from the GCD curves are listed in **Table S6**.

Table S6. C_m and C_v values of the oxygenic graphyne derived from CV and GCD curves.

Methods and experimental conditions		C_m (F g^{-1})	C_v (F cm^{-3})
GCD curves at different current densities (A g^{-1})	0.2	211.2	257.6
	0.5	188.0	229.3
	1	140.1	170.9
	2	136.2	166.1
	3	127.2	155.1
	10	113.1	137.9
	20	101.4	123.7
CV curves at different scan rates (mV s^{-1})	1	210.3	256.4
	2	197.8	241.2
	5	183.1	223.3
	10	172.9	210.8
	25	160.6	195.8
	50	149.9	182.8
	75	142.9	174.3
	100	137.5	167.7

C_m: gravimetric specific capacitance

C_v: volumetric specific capacitance

Table S7. Comparison of various carbon electrode materials for supercapacitors.

Carbon materials	Specific surface area ($m^2 g^{-1}$)	Capacitance in aqueous electrolyte		Cost	Ref.
		C_m ($F g^{-1}$)	C_v ($F cm^{-3}$)		
Carbon nanotubes	120–500	50–100	<60	High	1-3
Graphene	2630	100–205	------	High	4-6
Activated carbon	1000–3500	<200	<80	Low	7-9
Activated carbon fibers	1000–3000	120–370	<150	Medium	10-12
Carbon aerogels	400–1000	100–125	<80	Low	13-15
Graphyne	330–720	48–135	------	Medium	16-19
Graphdiyne	600–1300	<200	------	Medium	19-22
Naphyne	970.9	154	158.6	Low	23
OACM	686.9	121.8	166.6	Low	24
SACM	759.8	217.0	232.3	Low	25
NACM	578.3	215.6	292.9	Low	26
Oxygenic graphyne	**566.5**	**211.2**	**257.6**	**Low**	**This work**

C_m: gravimetric specific capacitance

C_v: volumetric specific capacitance

Table S8. The electrical conductivity performance of various carbon materials.

Carbon materials	Electrical conductivity (S m^{-1})	Ref.
Carbon black	100~10^4	27-30
CNT fibers	700~3000	31-34
CNT-graphene hybrid fibers	1200~10^4	4, 35-37
Graphene fibers	3500~10^5	5, 37-40
Graphene aerogel	<750	41-43
Graphene oxide papers	1350~10^4	38, 44, 45
Reduced graphene oxide	<1500	44-46
Activated carbon	<2000	8, 47, 48
Onion like carbons	<500	49-51
Graphdiyne	1900~10^4	20, 52-54
γ-Graphyne	200~5000	19, 55-58
Naphyne	1490	23
OACM	1522	24
NACM	1718	26
Oxygenic graphyne	**1866**	**This work**

References

1. Q. Wang, J. Yan and Z. Fan, Carbon materials for high volumetric performance supercapacitors: design, progress, challenges and opportunities, *Energ. Environ. Sci.*, 2016, **9**, 729-762.
2. Y. Wang, Y. Song and Y. Xia, Electrochemical capacitors: mechanism, materials, systems, characterization and applications, *Chem. Soc. Rev.*, 2016, **45**, 5925-5950.
3. K. Joseph, H. J. Kasparian and V. Shanov, *Energies*, 2022, **15**.
4. Z. Yang, J. Tian, Z. Yin, C. Cui, W. Qian and F. Wei, Carbon nanotube- and graphene-based nanomaterials and applications in high-voltage supercapacitor: a review, *Carbon*, 2019, **141**, 467-480.
5. X. Zheng, Q. Hu, X. Zhou, W. Nie, C. Li and N. Yuan, Graphene-based fibers for the energy devices application: A comprehensive review, *Mater. Design*, 2021, **201**, 109476.
6. J. Xiao, J. Han, C. Zhang, G. Ling, F. Kang and Q. Yang, Dimensionality, function and performance of carbon materials in energy storage devices, *Adv. Energy Mater.*, 2021, 2100775.
7. Y. He, X. Zhuang, C. Lei, L. Lei, Y. Hou, Y. Mai and X. Feng, Porous carbon nanosheets: synthetic strategies and electrochemical energy related applications, *Nano Today*, 2019.
8. L. Luo, Y. Lan, Q. Zhang, J. Deng, L. Luo, Q. Zeng, H. Gao and W. Zhao, A review on biomass-derived activated carbon as electrode materials for energy storage supercapacitors, *J. Energ. Stora.*, 2022, **55**, 105839.
9. C. Zhao, L. Ge, L. Mai, X. Li, S. Chen, Q. Li, S. Li, L. Yao, Y. Wang and C. Xu, Review on coal-based activated carbon: preparation, modification, application, regeneration, and perspectives, *Energ. Fuel*, 2023, **37**, 11622-11642.
10. S. Chen, L. Qiu and H. Cheng, Carbon-based fibers for advanced electrochemical energy storage devices, *Chem. Rev.*, 2020, **120**, 2811-2878.
11. T. Subramaniam, S.. Krishnan, M. Ansari, N. Hamid and M. Khalid, Recent progress on supercapacitive performance of agrowaste fibers: a review, *Crit. Rev. Solid State*, 2023, **48**, 289-331.

12. H. Zhou, Y. Su, J. Zhang, H. Li, L. Zhou and H. Huang, A novel embedded all-solid-state composite structural supercapacitor based on activated carbon fiber electrode and carbon fiber reinforced polymer matrix, *Chem. Eng. J.*, 2023, **454**, 140222.
13. Q. Dou, N. Wu, H. Yuan, K. Shin, Y. Tang, D. Mitlin and H. Park, Emerging trends in anion storage materials for the capacitive and hybrid energy storage and beyond, *Chem. Soc. Rev.*, 2021, **50**, 6734-6789.
14. C. Xiong, Y. Zhang and Y. Ni, Recent progress on development of electrolyte and aerogel electrodes applied in supercapacitors, *J. Power Sources*, 2023, **560**, 232698.
15. S Ashok Kumar, S. Bashir, M. Pershaanaa, F. Kamarulazam, N. Saidi, Z. Goh, I. Ma, V. Kunjunee, A. Jamaluddin, K. Ramesh, S. Ramesh, S. Ramesh and R. Manikam, A review on the recent progress of the plant-based porous carbon materials as electrodes for high-performance supercapacitors, *J. Mater. Sci.*, 2023, **58**, 6516-6555.
16. Y. Li, Q. Liu, W. Li, H. Meng, Y. Lu and C. Li, Synthesis and supercapacitor application of alkynyl carbon materials derived from CaC_2 and polyhalogenated hydrocarbons by interfacial mechanochemical reactions, *ACS Appl. Mater. Interfaces*, 2017, **9**, 3895-3901.
17. W. Ding, M. Sun, Z. Zhang, X. Lin and B. Gao, Ultrasound-promoted synthesis of γ-graphyne for supercapacitor and photoelectrochemical applications, *Ultrason. Sonochem.*, 2020, **61**, 104850.
18. M. Kenarsari, M. Vafaee, M. Nasrollahpour and S. Khoshdel, Evaluating the appropriateness of γ-graphyne derivatives as electrode materials for supercapacitors, *Sci. Rep.*, 2023, **13**, 15090.
19. H. Li, J. H. Lim, Y. Lv, N. Li, B. Kang and J. Lee, Graphynes and graphdiynes for energy storage and catalytic utilization: theoretical insights into recent advances, *Chem. Rev.*, 2023, **123**, 4795-4854.
20. X. Chen, X. Jiang and N. Yang, Graphdiyne electrochemistry: progress and perspectives, *Small*, 2022, **18**, 2201135.
21. D. Zhang, X. Li, W. Liu, J. Gao, X. Yan, Q. Liu and C. Huang, Research of graphdiyne materials applied for electrochemical energy storage, *Nano Trends*, 2023, **4**, 100017.

22. F. Wang, Z. Zuo, H. Shang, Y. Zhao and Y. Li, Ultrafastly interweaving graphdiyne nanochain on arbitrary substrates and its performance as a supercapacitor electrode, *ACS Appl. Mater. Interfaces*, 2019, **11**, 2599-2607.
23. Y. Li, Y. Li, P. Lin, J. Gu, X. He, M. Yu, X. Wang, C. Liu and C. Li, Architecture and electrochemical performance of alkynyl-linked naphthyl carbon skeleton: naphyne, *ACS Appl. Mater. Interfaces*, 2020, **12**, 33076-33082.
24. Y. Li, S. Li, X. Xu, J. Gu, X. He, H. Meng, Y. Lu and C. Li, Converting CO_2 into an oxygenated alkynyl carbon material with high electrochemical performance through a mechanochemical reaction with CaC_2, *ACS Sustain. Chem. Eng.*, 2021, **9**, 9221-9229.
25. Y. Li, X. Xu, B. Qiang, Y. Li, Y. Lu and C. Li, Turn hazardous endosulfan into S-doped alkynyl carbon material for energy storage and Hg(II) adsorption via a green mechanochemical process, *ACS Sustain. Chem. Eng.*, 2022, **10**, 9216-9224.
26. Y. Li, B. Qiang, X. Xu, Y. Li, J. Tang and C. Li, Mechanochemical degradation of hazardous pentachloronitrobenzene to in-situ N-doped alkynyl carbon material with high supercapacitor performance, *Appl. Surf. Sci.*, 2022, **604**, 154598-154606.
27. A. Motaghi, A. Hrymak and G. Motlagh, Electrical conductivity and percolation threshold of hybrid carbon/polymer composites, *J. Appl. Polym. Sci.*, 2015, **132**.
28. T. Silva, F. Moraes, B. Janegitz and O. Fatibello-Filho, Electrochemical biosensors based on nanostructured carbon black: a review, *J. Nanomater.*, 2017, **2017**.
29. M. Ali, L. Lin and D. Cartridge, High electrical conductivity waterborne dispersions of carbon black pigment, *Prog. Org. Coat.*, 2019, **129**, 199-208.
30. R. Kour, S. Arya, S. Young, V. Gupta, P. Bandhoria and A. Khosla, Review—recent advances in carbon nanomaterials as electrochemical biosensors, *J. Electrochem. Soc.*, 2020, **167**, 037555.
31. L. Kou, Y. Liu, C. Zhang, L. Shao, Z. Tian, Z. Deng and C. Gao, A mini review on nanocarbon-based 1D macroscopic fibers: assembly strategies and mechanical properties, *Nano-micro Lett.*, 2017, **9**, 51.

32. J. Wang, X. Luo, T. Wu and Y. Chen, High-strength carbon nanotube fibre-like ribbon with high ductility and high electrical conductivity, *Nat. Commun.*, 2014, **5**, 3848.
33. X. Zhang, W. Lu, G. Zhou and Q. Li, Understanding the mechanical and conductive properties of carbon nanotube fibers for smart electronics, *Adv. Mater.*, 2020, **32**, 1902028.
34. A. Kumar, K. Sharma and A. R. Dixit, A review on the mechanical properties of polymer composites reinforced by carbon nanotubes and graphene, *Carbon Lett.*, 2021, **31**, 149-165.
35. Z. Lu, J. Foroughi, C. Wang, H. Long and G. Wallace, superelastic hybrid CNT/graphene fibers for wearable energy storage, *Adv. Energy Mater.*, 2018, **8**, 1702047.
36. S. Pyo, Y. Eun, J. Sim, K. Kim and J. Choi, Carbon nanotube-graphene hybrids for soft electronics, sensors, and actuators, *Micro. Nano System. Lett.*, 2022, **10**, 9.
37. M. Islam, S. Afroj, M. Uddin, D. Andreeva, K. Novoselov and N. Karim, Graphene and CNT-based smart fiber-reinforced composites: a review, *Adv. Funct. Mater.*, 2022, **32**, 2205723.
38. A. Olabi, M. Abdelkareem, T. Wilberforce and E. Sayed, Application of graphene in energy storage device – a review, *Renew. Sustain. Energy Rev.*, 2021, **135**, 110026.
39. B. Fang, D. Chang, Z. Xu and C. Gao, A review on graphene fibers: expectations, advances, and prospects, *Adv. Mater.*, 2020, **32**, 1902664.
40. Y. Jia, J. Zhang, D. Kong, C. Zhang, D. Han, J. Han, Y. Tao, W. Lv and Q. Yang, Practical graphene technologies for electrochemical energy storage, *Adv. Funct. Mater.*, 2022, **32**, 2204272.
41. G. Gorgolis and C. Galiotis, Graphene aerogels: a review, *2D Mater.*, 2017, **4**, 032001.
42. Z. Cheng, R. Wang, Y. Wang, Y. Cao, Y. Shen, Y. Huang and Y. Chen, Recent advances in graphene aerogels as absorption-dominated electromagnetic interference shielding materials, *Carbon*, 2023, **205**, 112-137.
43. L. Cao, C. Wang and Y. Huang, Structure optimization of graphene aerogel-based composites and applications in batteries and supercapacitors, *Chem. Eng. J.*, 2023, **454**, 140094.
44. P. P. Brisebois and M. Siaj, Harvesting graphene oxide – years 1859 to 2019: a review of its structure, synthesis, properties and exfoliation, *J. Mater. Chem. C*, 2020, **8**, 1517-1547.

45. A. Zhou, J. Bai, W. Hong and H. Bai, Electrochemically reduced graphene oxide: preparation, composites, and applications, *Carbon*, 2022, **191**, 301-332.
46. L. Guex, B. Sacchi, K. Peuvot, R. Andersson, A. Pourrahimi, V. Ström, S. Farris and R. Olsson, Experimental review: chemical reduction of graphene oxide (GO) to reduced graphene oxide (rGO) by aqueous chemistry, *Nanoscale*, 2017, **9**, 9562-9571.
47. A. Barroso Bogeat, Understanding and tuning the electrical conductivity of activated carbon: a state-of-the-art review, *Crit. Rev. Solid State*, 2021, **46**, 1-37.
48. G. Reis, S. Larsson, H. Oliveira, M. Thyrel and E. Claudio Lima, Sustainable biomass activated carbons as electrodes for battery and supercapacitors-a mini-review, *Nanomater.*, 2020, **10**, 1398.
49. A. Borenstein, O. Hanna, R. Attias, S. Luski, T. Brousse and D. Aurbach, Carbon-based composite materials for supercapacitor electrodes: a review, *J. Mater. Chem. A*, 2017, **5**, 12653-12672.
50. V. Dhand, M. Yadav, S. Kim and K. Rhee, A comprehensive review on the prospects of multi-functional carbon nano onions as an effective, high- performance energy storage material, *Carbon*, 2021, **175**, 534-575.
51. A. Vindhyasarumi, K. Anjali, A. Sethulekshmi, J. Jayan, B. Deeraj, A. Saritha and K. Joseph, A comprehensive review on recent progress in carbon nano-onion based polymer nanocomposites, *Eur. Polym. J.*, 2023, **194**, 112143.
52. Z. Jia, Y. Li, Z. Zuo, H. Liu, C. Huang and Y. Li, Synthesis and properties of 2D carbon–graphdiyne, *Accounts Chem. Res.*, 2017, **50**, 2470-2478.
53. Y. Zhao, N. Yang, R. Yu, Y. Zhang, J. Zhang, Y. Li and D. Wang, Unique structural advances of graphdiyne for energy applications, *EnergyChem*, 2020, **2**, 100041.
54. G. Niu, Y. Wang, Z. Yang, S. Cao, H. Liu and J. Wang, Graphdiyne and its derivatives as efficient charge reservoirs and transporters in semiconductor devices, *Adv. Mater.*, 2023, **35**, 2212159.
55. M. Casco, F. Badaczewski, S. Grätz, A. Tolosa, V. Presser, B. Smarsly and L. Borchardt, Mechanochemical synthesis of porous carbon at room temperature with a highly ordered sp^2 microstructure, *Carbon*, 2018, **139**, 325-333.

56. Y. Song, X. Li, Z. Yang, J. Wang, C. Liu, C. Xie, H. Wang and C. Huang, A facile liquid/liquid interface method to synthesize graphyne analogs, *Chem. Commun.*, 2019, **55**, 6571-6574.
57. Y. Chen, X. Zhao, C. He, Q. Li and X. Cui, γ-Graphyne adjusted diffusion–capacitance behavior of lithium titanate for boosting high-rate and wide-temperature lithium storage, *J. Energy Storage*, 2023, **69**, 107920.
58. J. Wang, H. Shi, W. Wang, Z. Xu, C. Hong, Y. Xue and F. Tian, Defect engineering of graphynes for energy storage and conversion, *Chem. Eng. J.*, 2022, **432**, 133617.